IEEE Access
Multidisciplinary ⋮ Rapid Review ⋮ Open Access Journal

Received 19 December 2023, accepted 30 December 2023, date of publication 12 January 2024, date of current version 22 January 2024.

Digital Object Identifier 10.1109/ACCESS.2024.3353222

RESEARCH ARTICLE

Multi-Objective Optimization Technique Based on QUBO and an Ising Machine

HIROSHI IKEDA AND TAKASHI YAMAZAKI
Optimization Technology Project, Fujitsu Ltd., Kawasaki, Kanagawa 211-8588, Japan
Corresponding author: Hiroshi Ikeda (ikeike@fujitsu.com)

ABSTRACT With an increase in the complexity of society, solving multi-objective optimization problems (MOPs) has become crucial. In this study, we introduced a novel method called ''quadratic unconstrained binary optimization based on the weighted normal'' for solving MOPs using Ising machines, such as quantum annealing and digital annealer (DA), in the field of combinatorial optimization. The proposed method applies the penalty-based boundary intersection method to Ising machines under a setting limited to linear objective functions and maximizes the speed and performance of the DA, which is a quadratic unconstrained binary optimization-specific solver. We demonstrated the effectiveness of the proposed method by solving a real-world problem with a nonconvex shaped Pareto front (component combination problem). The results suggested that the proposed method could handle both convex- and nonconvex-shaped Pareto fronts, expanding the potential applications of Ising machines to solving complex MOPs. This development could significantly enhance decision-making processes, particularly in achieving sustainable development goals.

INDEX TERMS Multi-objective optimization, algorithm, combinatorial optimization.

I. INTRODUCTION

As society becomes increasingly complex, decision-making in corporate production activities and problem-solving requires a balance between multiple optimization indicators. For instance, achieving Goal 8 of Sustainable Development Goals – ''decent work and economic growth''– necessitates multi-objective solutions via mathematical optimization, which can be represented as follows:

$$\text{minimize} \quad \boldsymbol{F}(\boldsymbol{x}) = (f_1(\boldsymbol{x}), f_2(\boldsymbol{x}), \ldots, f_m(\boldsymbol{x})), \tag{1}$$

$$\text{subject to} \quad \boldsymbol{x} \in \Omega. \tag{2}$$

Here, we attempt to minimize the function $\boldsymbol{F}(\boldsymbol{x})$, which represents our objective, subject to certain constraints represented by $\boldsymbol{x}$ belonging to a set Ω. This is a common way to represent optimization problems mathematically. Here, $\boldsymbol{x}$ is the decision variable vector, Ω is the decision variable vector space, $f_i(\boldsymbol{x})$ is the i^{th} objective function; and $\boldsymbol{F}$ is the mapping from Ω to $\mathbf{R}^m$. $\mathbf{R}^m$ denotes the objective function vector space. $\boldsymbol{F}(\boldsymbol{x})$ is the objective function vector, and the set of attainable objective function vectors is $\{\boldsymbol{F}(\boldsymbol{x})|\boldsymbol{x} \in \Omega\}$. In multi-objective optimization problems (MOPs), the objective functions often conflict with each other. In such cases, improving one objective function degrades the other. Therefore, obtaining a balance between multiple objective functions in MOPs is necessary for an optimal solution, which is typically a set of solutions, called Pareto solutions, with trade-offs [1]. The set of objective function vectors corresponding to Pareto solutions in the objective function vector space is called the Pareto front (PF) [2].

In many applications of multi-objective optimization, decision-makers are interested in a set of Pareto solutions [3], [4]. Therefore, in continuous multi-objective optimization, methods for obtaining multiple Pareto solutions via multiple single-objective optimizations have been developed. A representative method is the weighted sum method [5], which involves constructing an objective function $E(\boldsymbol{x})$ from multiple objective functions $f_1(\boldsymbol{x})$, $f_2(\boldsymbol{x})$, $\ldots$, $f_m(\boldsymbol{x})$ via scalarization followed by optimization to obtain Pareto solutions. However, the weighted sum method cannot obtain sufficient Pareto solutions because the PF is nonconvex. To overcome this limitation, the Tchebycheff method [6],

The associate editor coordinating the review of this manuscript and approving it for publication was Mostafa M. Fouda.

normal boundary intersection (NBI) [7], penalty-based boundary intersection (PBI) [8], and Pareto adaptive PBI (PaP) [2] have been developed.

Quantum annealing has attracted attention as a single-objective optimization solver in combinatorial optimization [9], [10]. This method was inspired by quantum phenomena and has already been put into practical use [11], [12], [13]. Other optimization platforms that implement quantum annealing processing methods on digital systems, such as Fujitsu's digital annealer (DA) [14] and Hitachi's CMOS annealer [15], have also gained attention.

Quantum annealing formulates combinatorial optimization problems as an energy function called the Ising model. The Ising model links the values of variables with the up-spin and down-spin states and minimizes the energy function represented as a Hamiltonian via annealing processing. Quantum annealing and optimization platforms that use the quantum annealing processing methods described previously are collectively referred to as Ising machines. Replacing the spins of the Ising model with binary variables results in a quadratic unconstrained binary optimization (QUBO). Because the Ising model and QUBO are mutually convertible and equivalent, in this study, we used QUBO as a model that can be handled using Ising machines.

Single-objective optimization using QUBO (i.e., single-objective optimization that can be handled by Ising machines) is mathematically defined as follows:

$$\text{minimize} \quad f(\boldsymbol{x}) = \sum_{i=1}^{n}\sum_{j=1}^{n} G_{ij}x_i x_j \tag{3}$$

$$\text{subject to} \quad \boldsymbol{x} \in \{0,1\}^n. \tag{4}$$

Here, $\boldsymbol{G}$ is a two-dimensional matrix, and the objective function $f(\boldsymbol{x})$ is represented by QUBO using $\boldsymbol{G}$. G_{ij} is the element of $\boldsymbol{G}$. We attempt to minimize the function $f(\boldsymbol{x})$, which represents the energy of the system. $f(\boldsymbol{x})$ is subject to the constraint that $\boldsymbol{x}$ can only consider the values 0 or 1. This is a common approach to represent optimization problems in the context of quantum annealing. Here, $\boldsymbol{x} = (x_1, x_2, \ldots x_n)$ is the decision variable vector, which is a point in an n-dimensional discrete space with binary variables (0 or 1).

In the field of combinatorial optimization, several recent studies have investigated the solution of multi-objective optimization using Ising machines [16], [17], [18], [19]. These studies investigated the following problem settings on Ising machines, which are collectively called multi-objective unconstrained binary quadratic programming (mUBQP):

$$\text{minimize} \quad c_k(\boldsymbol{x}) = \sum_{i=1}^{n}\sum_{j=1}^{n} C_{ijk}x_i x_j, \quad \forall k \in \{1,2,\ldots,m\} \tag{5}$$

$$\text{subject to} \quad \boldsymbol{x} \in \{0,1\}^n. \tag{6}$$

Here, $\boldsymbol{C}$ is a three-dimensional matrix consisting of $m \times n \times n$ matrices, and C_{ijk} is the element of $\boldsymbol{C}$. In other words, it is a problem setting where each function c_k is QUBO. The mUBQP methods using the Ising model [16], [17], [18], [19] are similar to the previously described weighted sum method, where the weighted sum of objective functions $c_1, c_2, \ldots, c_m$ is used as the objective function and single-objective optimization is performed repeatedly. However, this method cannot obtain sufficient Pareto solutions when the PF is nonconvex.

In this study, we proposed a novel method that applies PBI using Ising machines under a problem setting limited to linear objective functions for the MOP. This method maximizes the speed and performance of the DA, a QUBO-specific solver [20], and obtains sufficient Pareto solutions even when the PF is nonconvex. We demonstrated the effectiveness of the proposed method by solving a real-world problem with a nonconvex-shaped PF, the component combination problem.

The remainder of this paper is organized as follows: In Section III, we explain the proposed method. In Section IV, we describe a simple problem that considers various PF shapes by changing only the constraints. In Section V, we present the results of the numerical experiments and the results of solving a newly given problem that is close to the actual field issues. Finally, in Section VI, we summarize the findings of this study.

II. RELATED RESEARCH

In this section, we discuss the research pertaining to the proposed method. First, we introduce the weighted sum method, Tchebycheff method [6], NBI [7], PBI [8], and PaP [2] in continuous MOPs and explain multi-objective optimization methods using Ising machines in combinatorial optimization.

A. OVERVIEW OF THE WEIGHTED SUM METHOD

The problem setting of the weighted sum method is defined as follows:

$$\text{minimize} \quad E^{WS}(\boldsymbol{x}|\boldsymbol{w}) = \sum_{i=1}^{m} w_i f_i(\boldsymbol{x}) \tag{7}$$

$$\text{subject to} \quad \boldsymbol{x} \in \Omega. \tag{8}$$

Here, $\boldsymbol{w} = (w_1, w_2, \ldots, w_m)$ is an m-dimensional weight vector. In addition, $\sum_{i=1}^{m} w_i = 1$, and $w_i \geq 0$ for each $i = 1, \ldots, m$. Pareto solutions are obtained by minimizing $E^{WS}(\boldsymbol{x}|\boldsymbol{w})$ for several $\boldsymbol{w}$ values. However, the weighted sum method cannot obtain sufficient Pareto solutions when the shape of the PF is nonconvex [21]. Methods such as the Tchebycheff method, NBI, PBI, and PaP have been developed to overcome this drawback.

B. OVERVIEW OF THE TCHEBYCHEFF METHOD

The problem setting of the Tchebycheff method is defined as follows:

$$\text{minimize} \quad E^{TE}(\boldsymbol{x}|\boldsymbol{w}, \boldsymbol{z}^*) = \max_{1\leq i\leq m} \left\{ w_i |f_i(\boldsymbol{x}) - z_i^*| \right\} \tag{9}$$

$$\text{subject to} \quad \boldsymbol{x} \in \Omega, \tag{10}$$

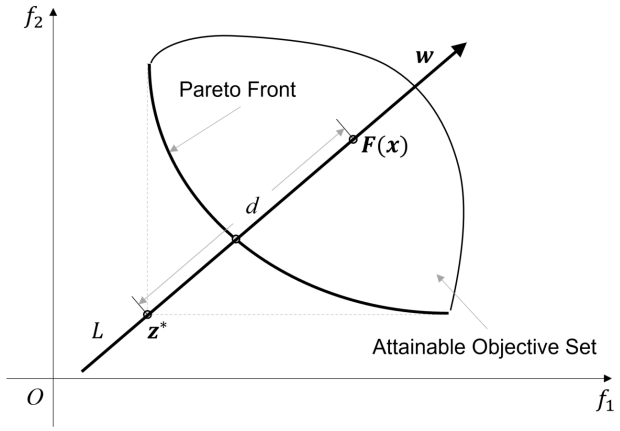

FIGURE 1. Illustration of the NBI approach (modified from [8]).

where $z^* = (z_1^*, \ldots, z_m^*)$ is the reference point. The reference point is a point in the objective function vector space consisting of the minimum values of each objective function in the MOP, where $z_i^* = \min\{f_i(x)|x \in \Omega\}$ for each $i = 1, \ldots, m$. w is the weight vector, as defined above. In the Tchebycheff method, Pareto solutions are obtained by minimizing $E^{TE}(x|w, z^*)$ for several w values.

C. OVERVIEW OF NBI

The problem setting of NBI is defined as follows:

$$\text{minimize} \quad E^{NBI}(x|w, z^*) = d \tag{11}$$
$$\text{subject to} \quad F(x) - z^* = dw, x \in \Omega. \tag{12}$$

Here, w and z^* are the weight vector and reference point, respectively, as previously defined. NBI minimizes $E^{NBI}(x|w, z^*)$ under the constraint $F(x) - z^* = dw$. Constraint $F(x) - z^* = dw$ restricts $F(x)$ to the line L passing through z^* in the w direction, as shown in Fig. 1. In NBI, Pareto solutions are obtained by minimizing $E^{NBI}(x|w, z^*)$ for several w values. In addition, the attainable objective shown in Fig. 1 represents the set of objective function vectors for constraint-satisfying solutions.

D. OVERVIEW OF PBI

PBI can be used to obtain Pareto solutions in continuous MOPs, even when the shape of the PF is nonconvex. The goal of the PBI is to identify points where a line extending from the reference point intersects the PF in the objective function vector space. The PBI problem setting is defined as follows:

$$\text{minimize} \quad E^{PBI}(x|w, z^*) = d_1 + \theta d_2 \tag{13}$$
$$\text{subject to} \quad x \in \Omega. \tag{14}$$

Here,

$$d_1 = \frac{\|(F(x) - z^*)^T w\|}{\|w\|}, \tag{15}$$
$$d_2 = \|F(x) - (z^* + d_1 w)\|. \tag{16}$$

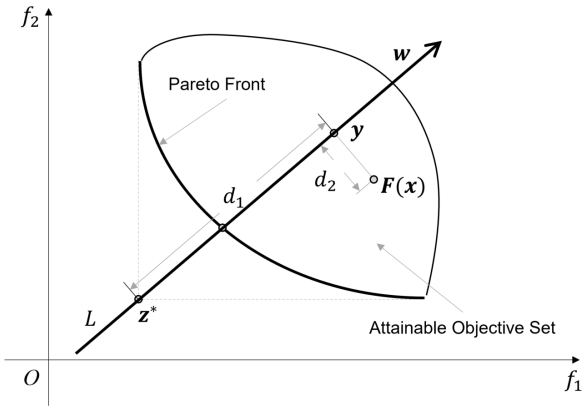

FIGURE 2. Illustration of the PBI approach (modified from [8]).

Here, $\theta > 0$ is the penalty parameter; when projecting $F(x)$ onto line L shown in Fig. 2, y is the projection; d_1 is the distance between z^* and y; d_2 is the distance between line L and $F(x)$; and θ is a parameter that balances d_1 and d_2 in $E^{PBI}(x|w, z^*)$. In the PBI, Pareto solutions can be obtained by minimizing $E^{PBI}(x|w, z^*)$ for several w values. However, PBI may not easily obtain Pareto solutions when the PF is nonconvex, although it exhibits good convergence when θ is small [22]. To address this issue, the PaP method is adopted, as it modifies θ accordingly. It is worth noting that a similar approach is adopted in the study of determining consensus in multiagent networks with constraints [23].

E. OVERVIEW OF OTHER MULTI-OBJECTIVE OPTIMIZATION METHODS USING ISING MACHINES FOR COMBINATORIAL OPTIMIZATION PROBLEMS

The solution methods using Ising machines for mUBQP [16], [17], [18], [19] minimize the following objective function $E(x|w)$ using the weight vector w for scalarization:

$$\text{minimize} \quad E(x|w) = \sum_{i=1}^{m} w_i c_i(x). \tag{17}$$

This scalarization is similar to that of the weighted sum method described above. Applying the Tchebycheff method, NBI, PBI, and PaP to Ising machines makes it difficult to obtain Pareto solutions even when the PF is nonconvex. This is because the maximum value operations, absolute values, and distance operations used in these methods cannot be processed by QUBO.

III. METHODS

A. PROBLEM SETTING OF MULTI-OBJECTIVE OPTIMIZATION

The problem setting of the MOP in the field of combinatorial optimization to be solved using the proposed method is as follows:

$$\text{minimize} \quad f_k(x) = \sum_{i=1}^{n} C_{ik} x_i + D_k, \ \forall k \in \{1, 2, \ldots, m\} \tag{18}$$
$$\text{subject to} \quad H_p(x) = 0, x \in \{0, 1\}^n. \tag{19}$$

Here, $H_p(\boldsymbol{x})$ is a nonlinear constraint represented in the form of QUBO, which is expressed as,

$$H_p(\boldsymbol{x}) = \sum_{i=1}^{n}\sum_{j=1}^{n} S_{ij}x_i x_j + K, \tag{20}$$

where $H_p(\boldsymbol{x}) \geq 0, \forall \boldsymbol{x}$. Furthermore, $\boldsymbol{C}$ is an $m \times n$ two-dimensional matrix and the objective function f_k is a linear expression with D_k as the constant term, as mentioned above. $\boldsymbol{S}$ is an $n \times n$ two-dimensional matrix, and K is a constant term. The constraints on the decision variable vector are described by H_p. In this MOP, the decision variable vector $\boldsymbol{x}$ was adjusted to optimize multiple objective functions. A solution refers to a decision variable vector $\boldsymbol{x}$ that satisfies the constraints and represents a point in the decision variable vector space. The decision variable vector space is the space of all possible values of $\boldsymbol{x}$. The objective function vector $\boldsymbol{F}(\boldsymbol{x}) = (f_1(\boldsymbol{x}), f_2(\boldsymbol{x}), \ldots, f_m(\boldsymbol{x}))$ corresponding to each $\boldsymbol{x}$ represents a point in the objective function vector space. Therefore, the goal of optimization is to select a point $\boldsymbol{x}$ in the decision variable vector space and optimize the point $\boldsymbol{F}(\boldsymbol{x})$ in the objective function vector space, thereby obtaining the PF.

B. SCALARIZATION IN QUBO BASED ON THE WEIGHTED NORMAL

We proposed a novel method, which we named QUBO weighted normal (QUBO-wN), that applies PBI using Ising machines. This method is specifically designed for problem settings limited to linear objective functions in the MOP. It utilizes the weight vector $\boldsymbol{w}$ and performs scalarization. The scalarized objective function is expressed as follows:

$$\text{minimize} \quad E(\boldsymbol{x}|\boldsymbol{w}) = H_s(\boldsymbol{x}|\boldsymbol{w}) + \xi H_d(\boldsymbol{x}|\boldsymbol{w}) + \lambda H_p(\boldsymbol{x}). \tag{21}$$

The first and second terms of (21), $H_s(\boldsymbol{x}|\boldsymbol{w}) + \xi H_d(\boldsymbol{x}|\boldsymbol{w})$, are the objective terms; the third term, $\lambda H_p(\boldsymbol{x})$, is the constraint term; and λ is a penalty parameter for the constraint term. The objective term is QUBO, which will be described later, and ξ is a parameter with a value greater than or equal to zero. Additionally, because the constraint term is a QUBO from the problem setting, the objective function $E(\boldsymbol{x}|\boldsymbol{w})$ in (21), which includes the constraint term, is a constrained QUBO. Constrained QUBO is an approach to solve combinatorial optimization problems, which is aimed at finding solutions that satisfy constraint conditions and is applied to optimization methods using quantum annealing and quantum computers [24]. The larger the penalty parameter λ, the greater the penalty for solutions that do not satisfy the constraint conditions, and the more likely it is to choose solutions that satisfy the constraints [20]. Moreover, the objective terms $H_s(\boldsymbol{x}|\boldsymbol{w})$ and $H_d(\boldsymbol{x}|\boldsymbol{w})$ are represented by the following expressions using the weight vector $\boldsymbol{w}$:

$$H_s(\boldsymbol{x}|\boldsymbol{w}) = \sum_{k=1}^{m} w_k f_k(\boldsymbol{x}), \tag{22}$$

$$H_d(\boldsymbol{x}|\boldsymbol{w}) = \sum_{k=1}^{m}\left(1 - \frac{w_k^2}{Z}\right)(f_k(\boldsymbol{x}))^2 - \frac{2}{Z}\sum_{k=1}^{m}\sum_{l>k}^{m} w_k w_l f_k(\boldsymbol{x}) f_l(\boldsymbol{x}). \tag{23}$$

Here, $Z = \sum_{k=1}^{m} w_k^2$. Because $f_k(\boldsymbol{x})$ is a linear expression with $x_i (i = 1, \ldots, n)$ as a variable, $H_s(\boldsymbol{x}|\boldsymbol{w})$ is a linear expression. Each element x_i of the decision variable vector $\boldsymbol{x}$ is a binary variable, and the identity equation $x_i^2 = x_i$ holds, as $H_s(\boldsymbol{x}|\boldsymbol{w})$ defined using (22) becomes a QUBO. Furthermore, for $H_d(\boldsymbol{x}|\boldsymbol{w})$ in (23), $(f_k(\boldsymbol{x}))^2$ and $f_k(\boldsymbol{x})f_l(\boldsymbol{x})$ are the most quadratic, and $H_d(\boldsymbol{x}|\boldsymbol{w})$, which is represented by their linear sum, becomes a QUBO.

C. BASIC CONCEPT OF QUBO-WN

To better understand the concept of QUBO-wN, it is essential to grasp the principles of multi-objective optimization and the weighted sum method. Multi-objective optimization involves optimizing multiple conflicting objectives simultaneously. In this study, we used a MOP with two objective functions. The weighted sum method is a common approach to this problem, where each objective is assigned a weight and the sum of these weighted objectives is minimized. We first discussed the weighted sum method related to $H_s(\boldsymbol{x}|\boldsymbol{w})$ in (22) and its drawbacks. Next, we explained the derivation of $H_d(\boldsymbol{x}|\boldsymbol{w})$ in (23), which extends the PBI.

In the weighted sum method, scalarization is performed using the weight vector $\boldsymbol{w}$ as follows:

$$E^{WS}(\boldsymbol{x}|\boldsymbol{w}) = w_1 f_1(\boldsymbol{x}) + w_2 f_2(\boldsymbol{x}). \tag{24}$$

Here, w_1 and w_2 are the weights assigned to the first and second objectives, respectively, and $f_1(\boldsymbol{x})$ and $f_2(\boldsymbol{x})$ are the values of these objectives for a given solution $\boldsymbol{x}$. The weighted sum method obtains multiple Pareto solutions by performing minimization multiple times while changing the weights w_1 and w_2 in (24) to satisfy $w_1 \geq 0$, $w_2 \geq 0$, $w_1 + w_2 = 1$. However, the weighted sum method cannot obtain sufficient Pareto solutions when the PF is nonconvex in the objective function vector space, as shown in Fig. 3, when it bulges to the upper right. The weighted sum method can obtain only two solutions: points A and B.

The part corresponding to the objective function in (24) is $H_s(\boldsymbol{x}|\boldsymbol{w})$ in (22) for the proposed method. With this part alone, similar to that in the weighted sum method, sufficient Pareto solutions cannot be obtained when the PF is nonconvex, which is a drawback. Therefore, in the proposed method, we incorporated the idea of including the distance d_2 between line l and point Q of the PBI in the objective function to obtain sufficient Pareto solutions even when the PF is nonconvex. Specifically, $H_d(\boldsymbol{x}|\boldsymbol{w})$ in (23) was added to the scalarized objective function to bring point Q in the objective function vector space shown in Fig. 3 closer to line l. Here, point Q is the point $\boldsymbol{F}(\boldsymbol{x}) = (f_1(\boldsymbol{x}), f_2(\boldsymbol{x}))$ in the objective function vector space, with coordinates corresponding to the pair of two objective function values

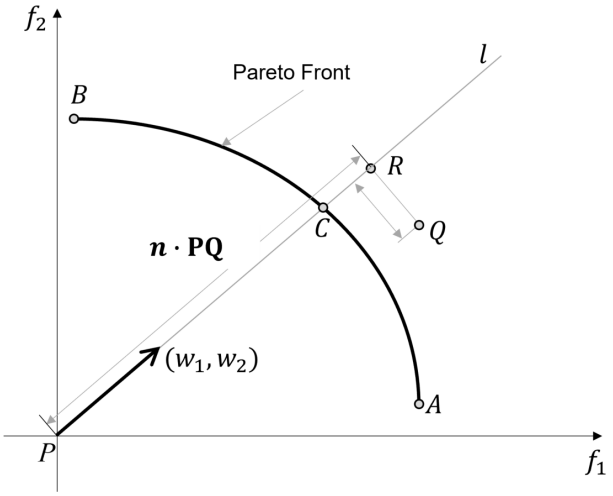

FIGURE 3. Schematic diagram around the PF of the nonconvex type.

for solution $\boldsymbol{x}$. Line l passed through point P in the objective function vector space and had $\boldsymbol{n}$ as the unit direction vector. The weight $\boldsymbol{w}$ vector determines the unit direction vector $\boldsymbol{n}$ as follows:

$$\boldsymbol{n} = \frac{1}{\sqrt{Z}}(w_1, w_2). \tag{25}$$

$H_d(\boldsymbol{x}|\boldsymbol{w})$ is defined as,

$$H_d(\boldsymbol{x}|\boldsymbol{w}) = |PQ|^2 - (\boldsymbol{n}\cdot PQ)^2. \tag{26}$$

If we add a perpendicular from point Q to line l and denote the foot of the perpendicular point R, H_d becomes the square of the distance between points R and Q, that is, the square of the distance between point Q and line l. H_d becomes smaller as point Q approaches line l. Assuming that $f_1(\boldsymbol{x}) \geq 0$ and $f_2(\boldsymbol{x}) \geq 0$ without the loss of generality, we set point P to have coordinates $(0, 0)$, and, because $\boldsymbol{n}$ is calculated using (25), we obtain

$$|PQ|^2 = (f_1(\boldsymbol{x}))^2 + (f_2(\boldsymbol{x}))^2, \tag{27}$$

$$(\boldsymbol{n}\cdot PQ)^2 = \frac{1}{Z}(w_1 f_1(\boldsymbol{x}) + w_2 f_2(\boldsymbol{x}))^2. \tag{28}$$

By incorporating (27) and (28) into (26), we obtained $H_d(\boldsymbol{x}|\boldsymbol{w})$, as shown in (29).

$$\begin{aligned} H_d(\boldsymbol{x}|\boldsymbol{w}) &= (f_1(\boldsymbol{x}))^2 + (f_2(\boldsymbol{x}))^2 \\ &\quad - \frac{1}{Z}(w_1 f_1(\boldsymbol{x}) + w_2 f_2(\boldsymbol{x}))^2 \\ &= \left(1 - \frac{w_1^2}{Z}\right)(f_1(\boldsymbol{x}))^2 + \left(1 - \frac{w_2^2}{Z}\right)(f_2(\boldsymbol{x}))^2 \\ &\quad - \frac{2}{Z} w_1 w_2 f_1(\boldsymbol{x}) f_2(\boldsymbol{x}). \end{aligned} \tag{29}$$

As mentioned earlier, H_d becomes a QUBO. For weights w_1 and w_2, the sum of (24) and ξH_d was used as the scalarized objective function. Similar to the weighted sum method, we adjusted the weights w_1 and w_2 to satisfy $w_1 \geq 0$, $w_2 \geq 0$, $w_1 + w_2 = 1$ and performed the optimization to obtain multiple Pareto solutions. While PBI includes the distance between line l and point Q in the scalarized objective function, the proposed method includes the square of the distance between line l and point Q in the scalarized objective function. By repeatedly optimizing the QUBO that brings point Q closer to the intersection of the line defined by the weight vector and PF, we obtained the Pareto solutions of the MOP. Owing to this characteristic, we named this method QUBO-wN.

Here, we considered H_d for the case in which the objective functions of the MOP are $m(\geq 3)$, as in the case with two objective functions. In this case, assuming that $f_k(\boldsymbol{x}) \geq 0$ $(k = 1, \ldots, m)$ without the loss of generality, we set point P as the origin in the objective function vector space under this assumption. Therefore, (25), (27), and (28) can be rewritten as follows:

$$\boldsymbol{n} = \frac{1}{\sqrt{Z}}(w_1, \ldots, w_m), \tag{30}$$

$$|PQ|^2 = \sum_{k=1}^{m} (f_k(\boldsymbol{x}))^2, \tag{31}$$

$$(\boldsymbol{n}\cdot PQ)^2 = \frac{1}{Z}\left(\sum_{k=1}^{m} w_k f_k(\boldsymbol{x})\right)^2. \tag{32}$$

By incorporating (31) and (32) into (26), H_d becomes:

$$\begin{aligned} H_d(\boldsymbol{x}|\boldsymbol{w}) &= \sum_{k=1}^{m}\left(1 - \frac{w_k^2}{Z}\right)(f_k(\boldsymbol{x}))^2 \\ &\quad - \frac{2}{Z}\sum_{k=1}^{m}\sum_{l>k}^{m} w_k w_l f_k(\boldsymbol{x}) f_l(\boldsymbol{x}). \end{aligned} \tag{33}$$

This is consistent with (23).

For the case where the objective functions of the MOP are $m(\geq 3)$, we generalized the above formulas. The unit direction vector $\boldsymbol{n}$ is expressed in (30), $|PQ|^2$ is the sum of the squares of the objective function values (31), and $(\boldsymbol{n}\cdot PQ)^2$ is the square of the weighted sum of the objective function values (32). By incorporating (31) and (32) into (26), $H_d(\boldsymbol{x}|\boldsymbol{w})$ becomes as shown in (33).

D. DETAIL PARAMETER DETERMINATION FOR EFFECTIVE SEARCH

Here, we explain the method for determining the parameter $\xi \geq 0$, which is included in the objective term of the scalarized QUBO used in the proposed method, using a MOP with two objective functions. The objective term mentioned earlier is denoted by H_{obj} as follows:

$$H_{obj}(\boldsymbol{x}|\boldsymbol{w}) = H_s(\boldsymbol{x}|\boldsymbol{w}) + \xi H_d(\boldsymbol{x}|\boldsymbol{w}). \tag{34}$$

To clarify the necessity of the parameter ξ, Figs. 4(a) and 4(b) show the contour lines connecting the same values of H_s and H_d in the objective function vector space when $f_1(\boldsymbol{x})$ and $f_2(\boldsymbol{x})$ both ranges from 0 to 5, respectively. The contour lines of H_s are perpendicular to the unit direction vector $\boldsymbol{n}$

determined by the weights w_1 and w_2, and we observed that H_s becomes smaller as we moved in the opposite direction of $\boldsymbol{n}$. Furthermore, from the contour lines of H_d, we observed that H_d decreases as it approaches the line extending from the origin in the $\boldsymbol{n}$ direction. Figures 4(c) and 4(d) show the contour lines of the objective term H_{obj} when $\xi = 1$ and 5, respectively. A comparison of these two figures showed that the spacing between the contour lines becomes narrower as ξ increased. In addition, focusing on the values of the objective term H_{obj} at points P_1 and P_2, we observed that H_{obj} is smaller at P_2 when $\xi = 1$ and at P_1 when $\xi = 5$. Thus, the relationship between the values of the objective term H_{obj} for the two points changed as ξ changed.

Considering the relationship between ξ and the values of the objective term H_{obj}, we determined the range of ξ based on a certain criterion. The criterion is as follows: ''When an unknown Pareto solution $\boldsymbol{x}$ exists on the line extending from point P in the $\boldsymbol{n}$ direction in the objective function vector space, the value of the objective term H_{obj} for that $\boldsymbol{x}$ is less than or equal to the value of the objective term H_{obj} for any 'known solution'.'' To clarify the procedure for determining the range of ξ that satisfies this criterion, we first defined the terms ''known solution,'' ''known nondominated solution,'' ''dominated region of the solution,'' ''dominated region boundary of the solution,'' ''dominated region of a nondominated solution set,'' and ''dominated region boundary of a nondominated solution set.''

Regarding the ''known solution,'' the proposed method repeats single-objective optimization by changing the weight vector, thereby providing solutions for the previous weight vectors, except for the first weight vector case. These solutions are called ''known solutions.'' Among the known solutions, if one solution is better in at least one objective function than other known solutions, the solution is considered a ''known nondominated solution.'' The ''dominated region of the solution'' is the region in the objective function vector space where all objective functions are worse than the values of objective functions of the solution. An example of the dominated region of solution $\boldsymbol{j}$ is shown in Fig. 5(a). The ''dominated region boundary of the solution'' is the boundary between the dominated region of the solution and other regions, as shown in Fig. 5(a). Figures 5(a) and 5(b) illustrate the objective function vector space. In this case, because both objective functions f_1 and f_2 are better when smaller, the region to the upper right from the objective function vector $\boldsymbol{F}(\boldsymbol{j})$ corresponding to solution $\boldsymbol{j}$ is the dominated region of solution $\boldsymbol{j}$. The ''dominated region of the nondominated solution set'' is the sum of dominated regions of each nondominated solution included in the nondominated solution set. An example of the dominated region of a nondominated solution set consisting of two nondominated solutions $\boldsymbol{j}_1$ and $\boldsymbol{j}_2$ is shown in Fig. 5(b). The region combining the upper-right areas of the objective function vectors $\boldsymbol{F}(\boldsymbol{j}_1)$ and $\boldsymbol{F}(\boldsymbol{j}_2)$ corresponding to solutions, $\boldsymbol{j}_1$ and $\boldsymbol{j}_2$ is the dominated region of the two nondominated solutions $\boldsymbol{j}_1$ and $\boldsymbol{j}_2$. The ''dominated region boundary of a nondominated solution set'' is the boundary between the dominated region of the nondominated solution set and other regions, as shown in Fig. 5(b).

Next, we explain the procedure for determining the range of ξ that satisfies the criteria under these definitions. First, we considered an unknown Pareto solution $\boldsymbol{x}$, on the line extending from point P in the $\boldsymbol{n}$ direction. Because points in the dominated region of the known nondominated solution set cannot be Pareto solutions, point X, whose coordinates are $(f_1(\boldsymbol{x}), f_2(\boldsymbol{x}), \ldots, f_m(\boldsymbol{x}))$, in the objective function vector space with coordinates of the objective function values at solution $\boldsymbol{x}$, must be outside the dominated region of the known nondominated solution set. Here, point T is the intersection of the boundary of the dominated region of the known nondominated solution set and the line extending from P in the $\boldsymbol{n}$ direction, with coordinates $(t_1, t_2, \ldots, t_m)$. If point X is on the opposite side of P from point T, $\boldsymbol{x}$ cannot be a Pareto solution. Therefore, point X must be on the same side of P as T.

Because the objective term H_{obj} and its elements H_s and H_d are the functions of both the decision variable and objective function vectors, Y_{obj}, Y_s, and Y_d hold the following relationships for all solutions $\boldsymbol{x}$:

$$H_{obj}(\boldsymbol{x}|\boldsymbol{w}) = Y_{obj}(X|\boldsymbol{w}), \tag{35}$$

$$H_s(\boldsymbol{x}|\boldsymbol{w}) = Y_s(X|\boldsymbol{w}), \tag{36}$$

$$H_d(\boldsymbol{x}|\boldsymbol{w}) = Y_d(X|\boldsymbol{w}). \tag{37}$$

Using the functions Y_{obj}, Y_s, and Y_d, the objective term at point T is $Y_{obj}(T|\boldsymbol{w})$, and the objective term at point $\boldsymbol{x}$ is $Y_{obj}(X|\boldsymbol{w})$. Because T and X are on the line extending from point P in the $\boldsymbol{n}$ direction, this is, on line l shown in Fig. 3, the value of Y_d is 0 for both points. Therefore, regardless of ξ,

$$Y_{obj}(T|\boldsymbol{w}) \geq Y_{obj}(X|\boldsymbol{w}). \tag{38}$$

Furthermore, let us assume that the set of known solutions as S and the objective term H_{obj} at solution $\boldsymbol{j}$ as $H_{obj}(\boldsymbol{j}|\boldsymbol{w})$. If

$$\forall \boldsymbol{j} \in S, \quad H_{obj}(\boldsymbol{j}|\boldsymbol{w}) \geq H_{obj}(\boldsymbol{x}|\boldsymbol{w}). \tag{39}$$

the value of H_{obj} for solution $\boldsymbol{x}$ is less than or equal to that of H_{obj} for all known solutions $\boldsymbol{j}$, and the criterion is satisfied. Based on (38) and (39), the sufficient condition for this is expressed as follows:

$$\forall \boldsymbol{j} \in S, \quad H_{obj}(\boldsymbol{j}|\boldsymbol{w}) \geq Y_{obj}(T|\boldsymbol{w}). \tag{40}$$

In the proposed method, we determined the range of ξ that satisfies (40).

The coordinates of point T can be calculated by identifying the set of nondominated solutions included in the existing solution set S and performing a geometric intersection calculation between the dominated region of the nondominated solution set in the objective function vector space and the line extending from point P in the $\boldsymbol{n}$ direction. From the coordinates of point T, the value of $Y_s(T|\boldsymbol{w})$ on the righthand side of (39) can be calculated. Because $\boldsymbol{F}(\boldsymbol{j})$ is known for solution $\boldsymbol{j}$ included in the known solution set S, $H_s(\boldsymbol{j}|\boldsymbol{w})$ and

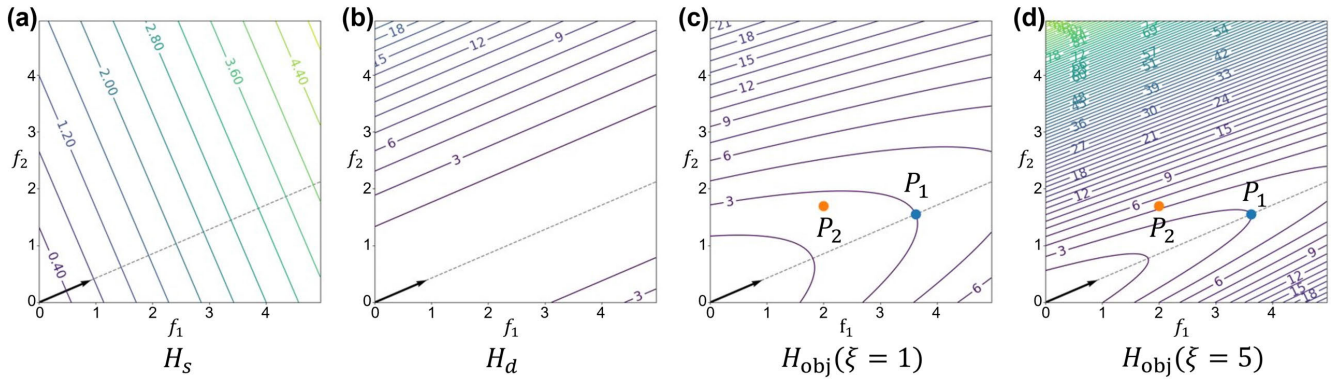

FIGURE 4. Contour maps of the respective objective functions under respective conditions.

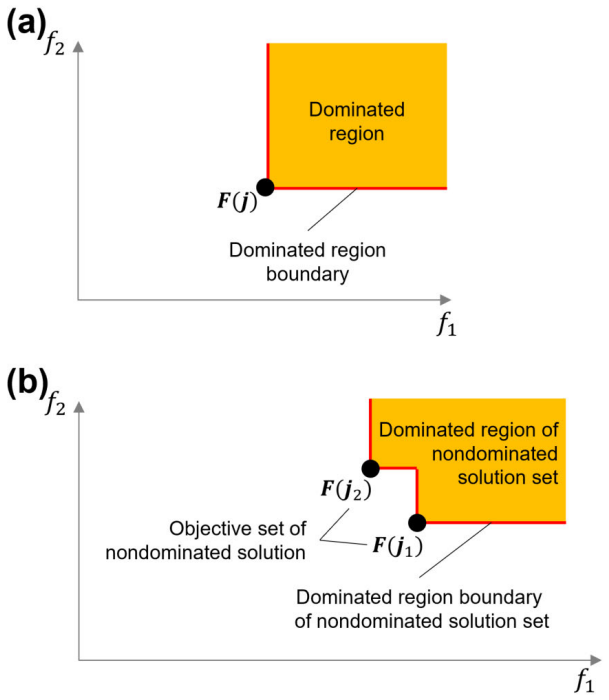

FIGURE 5. Schematic describing the technical terms used to determine the process of balanced parameters, ξ.

$H_d(\boldsymbol{j}|\boldsymbol{w})$ can be calculated. Because point T is on the line, $Y_d(T|\boldsymbol{w})$ is zero. Therefore, (40) is modified as follows:

$$\forall \boldsymbol{j} \in S, \quad H_s(\boldsymbol{j}|\boldsymbol{w}) + \xi H_d(\boldsymbol{j}|\boldsymbol{w}) \geq Y_s(T|\boldsymbol{w}). \tag{41}$$

If $H_d(\boldsymbol{j}|\boldsymbol{w})$ is 0, the objective function values for solution $\boldsymbol{j}$ are on the line extending from P in the $\boldsymbol{n}$ direction in the objective function vector space. Because T is a point on the boundary of the dominated region of the known nondominated solution set, solution $\boldsymbol{j}$ cannot be closer to point P than point T. Therefore, for solution $\boldsymbol{j}$ on the line, $H_{obj}(\boldsymbol{j}|\boldsymbol{w}) \geq Y_s(T|\boldsymbol{w})$ holds. However, if $H_d(\boldsymbol{j}|\boldsymbol{w})$ is not 0, (41) can be transformed, considering that $H_d(\boldsymbol{j}|\boldsymbol{w}) > 0$ according to (26), as follows:

$$\forall \boldsymbol{j}(\boldsymbol{j} \in S \wedge H_d(\boldsymbol{j}|\boldsymbol{w}) \neq 0), \quad \xi \geq \frac{H_s(\boldsymbol{x}|\boldsymbol{w}) - H_s(\boldsymbol{j}|\boldsymbol{w})}{H_d(\boldsymbol{j}|\boldsymbol{w})}. \tag{42}$$

Let S_d be the set of solutions in the known solution set S with nonzero H_d values, and let ξ_{th} be the smallest ξ satisfying (42). This is calculated as follows:

$$\xi_{th} = \max_{j \in S_d} \frac{Y_s(T|\boldsymbol{w}) - H_s(\boldsymbol{j}|\boldsymbol{w})}{H_d(\boldsymbol{j}|\boldsymbol{w})}. \tag{43}$$

Thus, the range $\xi \geq \xi_{th}$ satisfies the criterion, and this range of ξ was used in the proposed method.

However, there may be cases where the intersection of the dominated region boundary of the nondominated solution set and the line extending from point P in the $\boldsymbol{n}$ direction does not exist depending on $\boldsymbol{n}$. In such cases, as the range of ξ cannot be determined using the above criterion, we used the distance to the farthest point from point P among the points in the objective function space corresponding to the existing nondominated solutions. We then determined the range of ξ using the point on the line extending from point P in the $\boldsymbol{n}$ direction at that distance as a substitute for point T. Furthermore, for the first weight vector case, as there are no known solutions and the range of ξ cannot be determined using the above criterion, the range of ξ was set to be greater than or equal to 0.

Let us consider a scenario where we have a known solution set S as follows:

$$S = \{\boldsymbol{j}_1, \boldsymbol{j}_2, \boldsymbol{j}_3, \ldots, \boldsymbol{j}_m\}. \tag{44}$$

First, we identified the intersection point T of the line extending from point P in the $\boldsymbol{n}$ direction and the boundary of the dominated region of the known nondominated solution set. Next, for each solution $\boldsymbol{j}_i$, the values of the objective functions $H_s(\boldsymbol{j}_i|\boldsymbol{w})$ and $H_d(\boldsymbol{j}_i|\boldsymbol{w})$ were calculated. Let us assume these values are expressed as follows:

$$H_s(\boldsymbol{j}_1|\boldsymbol{w}) = 1.0, \quad H_d(\boldsymbol{j}_1|\boldsymbol{w}) = 0.5 \tag{45}$$

$$H_s(\boldsymbol{j}_2|\boldsymbol{w}) = 0.8, \quad H_d(\boldsymbol{j}_2|\boldsymbol{w}) = 0.6 \tag{46}$$

$$H_s(\boldsymbol{j}_3|\boldsymbol{w}) = 0.9, \quad H_d(\boldsymbol{j}_3|\boldsymbol{w}) = 0.7 \tag{47}$$
$$H_s(\boldsymbol{j}_4|\boldsymbol{w}) = 0.7, \quad H_d(\boldsymbol{j}_4|\boldsymbol{w}) = 0.0$$
$$\cdots \tag{48}$$

Then, we identify the set S_d of solutions in the known solution set S for which H_d is not zero. In this example, let us assume $S_d = \{\boldsymbol{j}_1, \boldsymbol{j}_2, \boldsymbol{j}_3\}$.

Next, we calculate ξ_{th} using (43). In this example, ξ_{th} is calculated as follows:

$$\xi_{th} = \max\left\{\frac{Y_s(T|\boldsymbol{w}) - H_s(\boldsymbol{j}_1|\boldsymbol{w})}{H_d(\boldsymbol{j}_1|\boldsymbol{w})}, \frac{Y_s(T|\boldsymbol{w}) - H_s(\boldsymbol{j}_2|\boldsymbol{w})}{H_d(\boldsymbol{j}_2|\boldsymbol{w})}, \frac{Y_s(T|\boldsymbol{w}) - H_s(\boldsymbol{j}_3|\boldsymbol{w})}{H_d(\boldsymbol{j}_3|\boldsymbol{w})}\right\} \tag{49}$$

Therefore, the range of ξ is $\xi \geq \xi_{th}$. This range was used in the proposed method. However, at the beginning, there are no known solutions; hence, the intersection point T does not exist. Therefore, the range of ξ is set to be greater than or equal to 0. Furthermore, the pseudocode for the process of determining the range of ξ is provided in the Appendix A.

IV. PROBLEM SETTING

The primary purpose of this study was to confirm that sufficient Pareto solutions could be obtained for MOPs with nonconvex PF shapes using the proposed method. In addition, because the shape of the PF is convex or nonconvex in real-world MOPs, the objective of the experiment was to confirm that sufficient Pareto solutions could be obtained for MOPs with either PF shape using the developed method.

In this study, we created a MOP in which the PF can be either convex or nonconvex based on imposing constraints. We used the following objective functions:

$$f_1(x_1, x_2) = x_1 + x_2 + 5, \tag{50}$$
$$f_2(x_1, x_2) = -x_1 + x_2 + 20. \tag{51}$$

Here, the range of the input variables is $x_i \in [0, 15]$, and all x_i are integers. In this MOP, the PF can be made convex by imposing the following constraints:

$$0.5\,x_1 + x_2 - 4 \geq 0, \tag{52}$$
$$-0.5\,x_1 + x_2 + 3.5 \geq 0. \tag{53}$$

Conversely, the PF can be made nonconvex by changing the constraints as follows:

$$(0.5\,x_1 + x_2 - 11.5 \geq 0) \vee (-0.5\,x_1 + x_2 - 4 \geq 0). \tag{54}$$

Considering that the constraints having an OR relationship (i.e., at least one of (54) must hold) results in a nonconvex MOP. Hereafter, the MOP with constraints (52) and (53) is referred to as problem 1, and the MOP with constraint (54) is referred to as problem 2.

Figure 6 shows the objective function vectors of constraint-satisfying solutions for all combinations of x_1 and x_2, where each vector ranged between 0 and 15, represented as points on a scatter plot in the objective function vector space. Figure 6(a) shows the points of the objective function vectors of constraint-satisfying solutions for problem 1, and Fig. 6(b) shows the points of objective function vectors of the constraint-satisfying solutions for problem 2. In Figs. 6(a) and 6(b), the points corresponding to the objective function vectors of Pareto solutions are indicated by light blue markers and the points corresponding to the objective function vectors of constraint-satisfying solutions other than Pareto solutions are indicated by green markers. Figures 6(a) and 6(b) indicate that the PF shapes of problems 1 and 2 are convex and nonconvex, respectively.

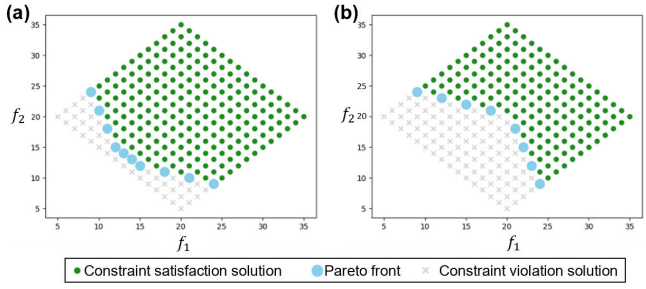

FIGURE 6. Problem settings of PFs of (a) convex and (b) nonconvex shapes.

V. RESULTS AND DISCUSSION

A. NUMERICAL RESULTS OBTAINED BY THE MIP SOLVER

First, we executed the weighted sum method represented in (53) using a known mixed integer programming (MIP) solver. The weights w_1 and w_2 were changed in increments of 0.02 to satisfy $w_1 \geq 0$, $w_2 \geq 0$, and $w_1 + w_2 = 1$. The representation for handling the OR constraint of problem 2 in the MIP solver is explained in Appendix B. Figure 7 shows the points corresponding to the objective function vectors of the solutions obtained using the MIP solver, added to Fig. 6 as yellow markers. Problems 1 and 2 are shown in Figs. 7(a), and Fig. 7(b), respectively. Notably, 5 of 10 Pareto solutions were obtained in problem 1, whereas, 2 of 8 Pareto solutions were obtained in problem 2. As expected, in problem 1 (with a convex PF shape), the obtained solution objective function vectors were distributed in several regions on the PF, whereas, in problem 2 (with a nonconvex PF shape), only the two points at both ends of the PF could be obtained. Of note, the objective function vectors of the solutions obtained by the weighted sum method using the DA were consistent with those shown in Fig. 7.

In problems 1 and 2, as the decision variables are integer variables, we converted integer variables to binary variables using binary expansion — a general method for representing problems with integer variables in the QUBO format [25]. Subsequently, we executed the weighted sum method using the DA. Inequality constraints were processed using the inequality constraint input function of the DA [20].

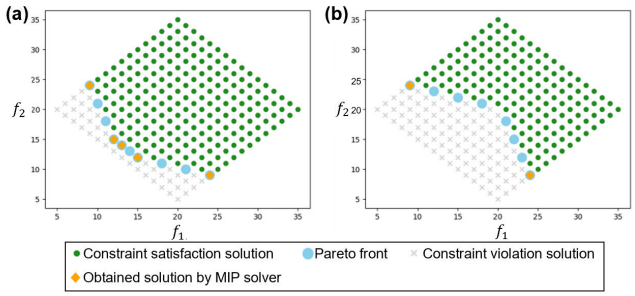

FIGURE 7. Results obtained by the MIP solver for (a) convex and (b) nonconvex PFs.

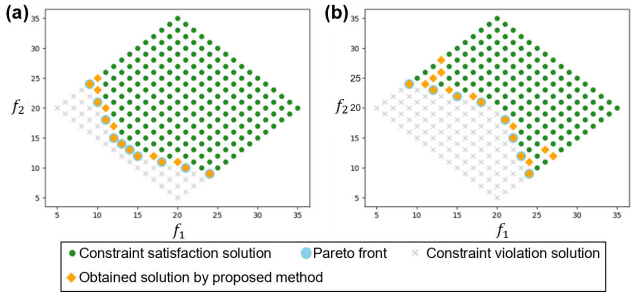

FIGURE 8. Results obtained by the QUBO-wN solver for a PF of (a) convex and (b) nonconvex shapes.

B. NUMERICAL RESULTS OBTAINED BY QUBO-WN

Using the binary expansion method [25] and the inequality constraint input function of the DA [20], we executed the proposed method for problems 1 and 2. The results for problems 1 and 2 are shown in Figs. 8(a) and 8(b), respectively. The points indicated by orange triangles in each figure correspond to the objective function vectors of the solutions obtained by the proposed method using the DA. When compared with Fig. 7(a), we confirmed that 10 Pareto solutions and 14 other solutions are obtained for the convex-shaped problem. On the other hand, when compared with Fig. 7(b), 8 Pareto solutions and 16 other solutions are obtained for the nonconvex-shaped problem. Thus, the proposed method can obtain sufficient Pareto solutions for both PF shapes.

In problems 1 and 2, we used a narrow range of problem settings, with x_i ranging from 0–15, to demonstrate that sufficient Pareto solutions can be obtained using the proposed method. Next, we created problems 3, 4, and 5 to investigate whether sufficient Pareto solutions can be obtained when x_i ranged from 0–255 and for more complex PF shapes. The objective functions for problems 3, 4, and 5 were the same and are expressed as follows:

$$f_1(x_1, x_2) = x_1 + x_2, \tag{55}$$
$$f_2(x_1, x_2) = -x_1 + x_2 + 255. \tag{56}$$

To shape the PF according to the problem, the constraints for problems 3, 4, and 5 are expressed in (57), (58), and (59), respectively, as follows:

$$\begin{aligned}&(0.5x_1 + x_2 - 74 \geq 0)\\ &\wedge (-0.5x_1 + x_2 + 53 \geq 0)\\ &\wedge (-0.25x_1 + x_2 - 62 \geq 0)\\ &\wedge (0.5x_1 + x_2 - 144 \geq 0),\end{aligned} \tag{57}$$
$$(0.5x_1 + x_2 - 144 \geq 0) \vee (-0.5x_1 + x_2 - 17 \geq 0), \tag{58}$$
$$\begin{aligned}&[(0.5x_1 + x_2 - 74 \geq 0) \wedge (-0.5x_1 + x_2 + 53 \geq 0)]\\ &\vee (0.5x_1 + x_2 - 144 \geq 0)\\ &\vee (-0.5x_1 + x_2 - 17 \geq 0).\end{aligned} \tag{59}$$

The results for problems 3, 4, and 5 using the proposed method are shown in Figs. 9(a), 9(b), and 9(c), respectively. The figures represent the objective function vector spaces of each problem, with the regions corresponding to the objective function vectors of constraint-satisfying solutions shown in blue as well as the regions corresponding to the objective function vectors of constraint-violating solutions shown in red. PF is indicated in light blue. From Fig. 9(c), we confirmed that the PF of problem 5 has a complex shape, similar to the two concave shapes that are connected. In each figure, the points corresponding to the objective function vectors of the Pareto solution obtained using the proposed method are indicated by orange markers. The results for 101 repetitions with different weights are shown, and Pareto solutions or solutions near the PF were obtained for problems 3, 4, and 5.

For a quantitative evaluation, we compared the PF shape obtained using the proposed method and the true PF obtained through the exhaustive search of all combinations of decision variables using the hypervolume [26]. The results indicated that the proposed method obtained PFs with hypervolume values of 99% or more compared with the true PF.

C. NUMERICAL RESULTS OF THE PARTS-COMBINATION PROBLEM

In this study, we addressed the component combination optimization problem in manufacturing as a real-world problem to which the proposed method must be applied. The problem setting for the component combination optimization problem is explained in this section. A single product consists of multiple functions and there are multiple candidate components for each function. The corresponding function is realized by selecting and implementing one component among the component candidates. The product is completed when all functions are realized. In this case, we set two objective functions with a trade-off relationship. For example, the purchase cost and production difficulty in assembly production can be considered objective functions. When changing to a lower-cost component, the difficulty of assembly production may increase. Because the selection of components affects the values of each objective function, selecting components that optimize the purchase cost and production difficulty when assembling the product is crucial. We assumed an exclusive constraint in which only one

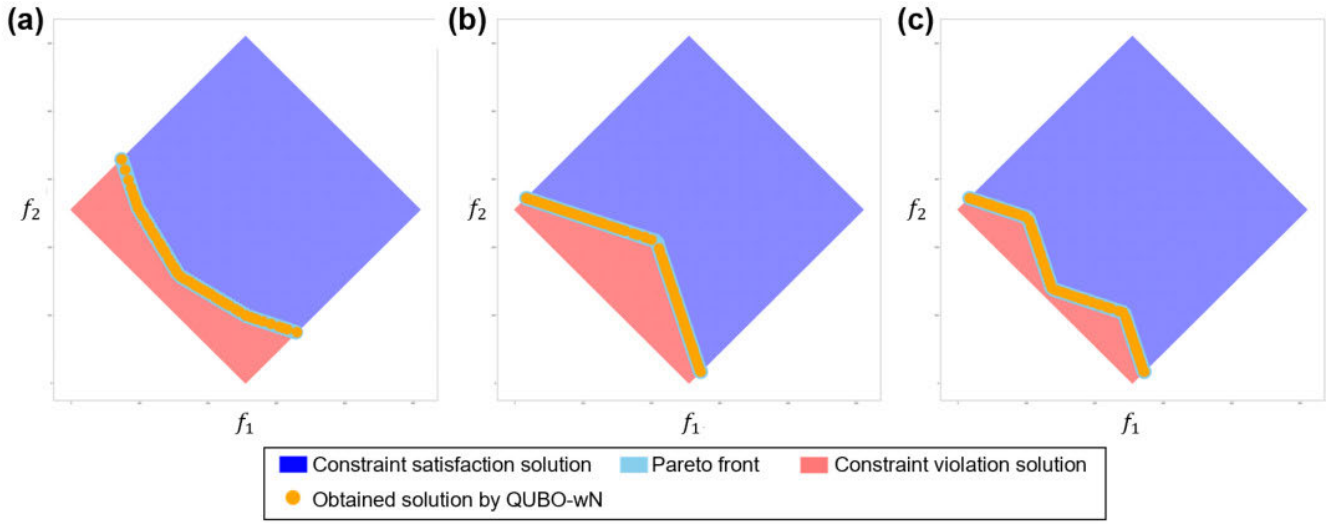

FIGURE 9. Results obtained by the QUBO-wN solver for problems 3, 4, and 5.

component can be selected among the candidate components for each function. We also assumed an exclusive constraint between the components of different functions, where, if component a_i of function α is selected, component b_j of another function β cannot be selected. This constraint arises when components a_i and b_j cannot be implemented in the productowing to the positional interference between the two components. Under these two constraints, that is, the constraint between components within the same function and the constraint between the components of different functions, the two objective functions were optimized. The two objective functions are represented by the following equations:

$$f_1 = \sum_i \sum_j a_{ij} x_{ij}, \tag{60}$$

$$f_2 = \sum_i \sum_j b_{ij} x_{ij}. \tag{61}$$

Here, f_1 and f_2 represent the two objective functions; x_{ij} is a binary variable representing the selection/non-selection of the j^{th} component of the i^{th} function; and a_{ij} and b_{ij} are coefficients representing the contribution of the j^{th} component of the ith function to f_1 and f_2, respectively. The shape of the PF of the component combination optimization problem is not necessarily nonconvex; however, a component combination optimization problem with a nonconvex PF shape can be created depending on the constraints between the two components and the magnitude of the contribution of each component to the two objective functions. In this study, we created a problem in which the shape of the PF is expected to be nonconvex and solved the problem using the proposed method.

To create a certain product, all functions can be covered by components from Company A; however, some or all components of the functions can be replaced with compatible components from Company B. Replacing the components may improve or worsen objective functions 1 and/or 2. Moreover, some or all components of the functions can be replaced with compatible components from Company C, but components from Companies B and C are not compatible and cannot coexist in the product. Some or all functional components can be replaced with compatible components from Company D, and components from Companies A, C, and D can coexist in the product. Components from Company D can be replaced with those from Company E, but components from Company E are not compatible with those from Companies A, B, and C and cannot coexist in the product.

TABLE 1. List of interrelationships between the companies.

	A	B	C	D	E
A	–	○	○	○	×
B	○	–	×	×	×
C	○	×	–	○	×
D	○	×	○	–	○
E	×	×	×	○	–

The objective function vectors using components from only one of Companies A–E are represented by the values at the positions labeled A to E in Fig. 10, which represents the objective function vector space. The objective function vectors for cases where components from Companies A and B are mixed, components from Companies A, C, and D are mixed, and products from Companies D and E are mixed, corresponding to the regions shown in Fig. 10. The shape of the PF was expected to be nonconvex. The compatibility and incompatibility of mixing components from Companies A–E are represented by inter-component constraints between different functions, and inter-component constraints are set for pairs of companies marked with "×" in Table 1.

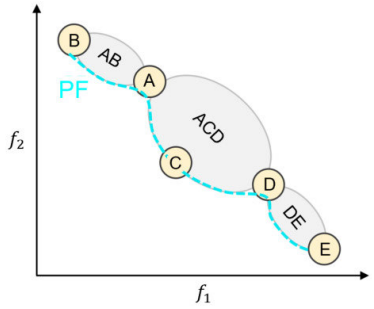

FIGURE 10. Schematic diagram showing the solutions of the parts-combination optimization problem with intercompany relationships.

Next, we considered a component combination optimization problem for a product with 10 functions and components from each of the five Companies A–E for each function. The two coefficients a_{ij} and b_{ij} were randomly set around the coordinates of Companies A–E as shown in Fig. 10, for the generation of experimental data. Figure 11(a) shows the region corresponding to the objective function vectors obtained by exhaustively enumerating the component selection combinations. The regions of the objective function vectors of constraint-violating solutions owing to compatibility issues between the components are indicated by red markers, and the objective function vectors of constraint-satisfying solutions are indicated by blue markers. Figure 11(a) shows that the PF has two connected concave shapes, as expected in Fig. 10. The points corresponding to the objective function vectors of the solutions obtained by the proposed method using the DA are shown in Fig. 11(b). Figure 11(b) shows that the proposed method can identify Pareto solutions, even when the PF has a connected concave shape. The results of the proposed method for an expanded problem with 200 functions are shown in Fig. 11(c). Even for large-scale problems, the proposed method can identify PFs with connected concave shapes, thereby confirming its effectiveness.

VI. CONCLUDING REMARK

In this study, we proposed QUBO-wN as a method for solving the PF of MOPs using Ising machines. This method involves performing single-objective optimization repeatedly to minimize a QUBO that includes the weighted sum of the objective function values as well as the distance between the objective function values and a line that varies according to the weights. The methods for solving the PF of MOPs using single-objective optimization have been investigated; however, scalarization techniques, such as the weighted sum method, cannot easily solve PFs with nonconvex shapes, leading to the development of methods such as the PBI. The proposed method is an application of PBI to MOPs in the combinatorial field using Ising machines, which can quickly solve the QUBO for single-objective optimization processes and PFs with convex and nonconvex shapes. The effectiveness of the proposed method was verified via numerical analyses. By solving the PF of a MOP in component combination as a real-world problem, its ability to solve even complex-shaped PFs was confirmed. From this result, we believed that this development could significantly enhance decision-making processes, particularly in achieving sustainable development goals. However, this study has some limitations. Currently, Ising machines only support QUBO, limiting the MOPs that can be solved using the proposed method to those with linear objective functions. This limitation must be addressed in a future work. However, if Ising machines are able to handle higher-order problems in the future, they will resolve combinatorial MOPs with higher-order objective functions. This is a promising direction for future research. Furthermore, the exploration of other scalarization techniques and their application to MOPs using Ising machines could also be a potential area of future investigation.

APPENDIX A
PSEUDOCODE FOR DETERMINING THE RANGE OF ξ

The algorithm for determining the range of ξ is described in detail as follows:

Algorithm 1 Range_of_xi

Input: $P, \boldsymbol{n}, S$
Output: ξ_{range}

1: **if** len$(S) == 0$ **then**
2: $\quad \xi_{range} \leftarrow [0, \infty]$
3: **else**
4: $\quad$ # Calculate the intersection point T by function of calculate_intersection_point.
5: $\quad T \leftarrow$ calculate_intersection_point$(P, \boldsymbol{n}, S)$
6: $\quad$ # Calculate $Y_s(T|\boldsymbol{w})$
7: $\quad \mathrm{YST} \leftarrow \sum_{k=1}^{m} w_k t_k$
8: $\quad \xi_{th} \leftarrow -\infty$
9: $\quad$ **for** each $\boldsymbol{j}_i$ in S **do**
10: $\quad\quad H_s \leftarrow \sum_{k=1}^{m} w_k f_k(\boldsymbol{j}_i)$
11: $\quad\quad H_d \leftarrow \sum_{k=1}^{m} \left(1 - \frac{w_k^2}{Z}\right) - \frac{2}{Z} \sum_{k=1}^{m} \sum_{l>k}^{m} w_k w_l f_k(\boldsymbol{j}_i) f_l(\boldsymbol{j}_i)$
12: $\quad\quad$ **if** $H_d == 0$ **then**
13: $\quad\quad\quad$ continue
14: $\quad\quad$ **end if**
15: $\quad\quad \xi_{th} \leftarrow \max\left(\xi_{th}, \frac{YST - H_s}{H_d}\right)$
16: $\quad$ **end for**
17: $\quad \xi_{range} \leftarrow [\xi_{th}, \infty]$
18: **end if**
19: **return** ξ_{range}

The function calculate_intersection_point$(P, \boldsymbol{n}, S)$ on line 5 computes the intersection coordinate $T = (t_1, t_2, \ldots, t_m)$ between the boundary of the dominated region of the known nondominated solution set and the line extending from P in the $\boldsymbol{n}$ direction.

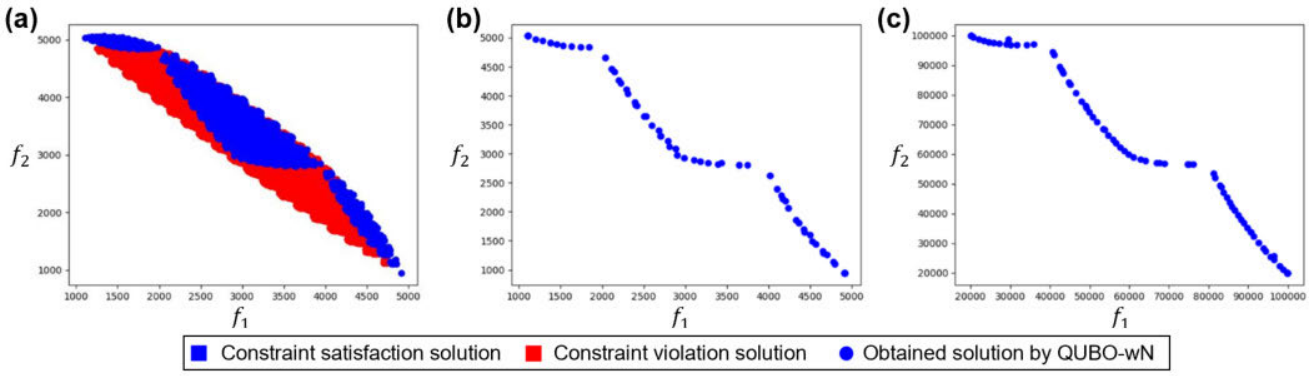

FIGURE 11. Problem setting and results obtained by the QUBO-wN solver for the parts-combination problem.

APPENDIX B
HANDLING CONSTRAINTS WITH OR RELATIONS IN THE MIXED INTEGER PROGRAMMING SOLVER USING THE BIG M METHOD

MIP is a method for solving optimization problems that combines continuous and integer variables. MIP solvers generally process constraint conditions that are expressed as linear inequalities and equations. These constraints must all be satisfied simultaneously because they are connected by AND relations. However, MIP solvers can also handle constraints with OR relationships. In this appendix, we explained how to handle constraints with OR relations in MIP solvers using the Big M method.

The Big M method introduces a sufficiently large value (Big M) into the constraint conditions and controls whether each constraint condition is satisfied by binary variables. For example, to handle the OR relation constraint of (54) in an MIP solver, we introduced the binary variables z_1 and z_2 and transformed them as follows:

$$0.5\,x_1 + x_2 - 11.5 \geq -M(1 - z_1), \tag{62}$$
$$-0.5\,x_1 + x_2 - 4 \geq -M(1 - z_2), \tag{63}$$
$$z_1 + z_2 \geq 1, \tag{64}$$

where, M is a sufficiently large positive value. This allows a solution to be obtained when at least one of the constraints in (62) or (63) is satisfied.

Furthermore, the constraint with mixed AND and OR relations in (59) can also be transformed using the Big M method by introducing binary variables $z_1, z_2, \ldots, z_5$ as follows:

$$0.5\,x_1 + x_2 - 74 \geq -M(1 - z_1), \tag{65}$$
$$-0.5\,x_1 + x_2 + 53 \geq -M(1 - z_2), \tag{66}$$
$$z_1 + z_2 - 1 \leq z_5, \tag{67}$$
$$z_5 \leq z_1, \tag{68}$$
$$z_5 \leq z_2, \tag{69}$$
$$0.5x_1 + x_2 - 144 \geq -M(1 - z_3), \tag{70}$$
$$-0.5x_1 + x_2 - 17 \geq -M(1 - z_4), \tag{71}$$
$$z_3 + z_4 + z_5 \geq 1. \tag{72}$$

As described above, MIP solvers can handle constraints with OR relations using the Big M method.

ACKNOWLEDGMENT

The authors would like to thank Editage (www.editage.jp) for English language editing.

REFERENCES

[1] E. Zitzler and L. Thiele, "Multiobjective optimization using evolutionary algorithms—A comparative case study," in *Proc. Int. Conf. Parallel Problem Solving From Nature*. Berlin, Germany: Springer, 1998, pp. 292–301.
[2] M. Ming, R. Wang, Y. Zha, and T. Zhang, "Pareto adaptive penalty-based boundary intersection method for multi-objective optimization," *Inf. Sci.*, vol. 414, pp. 158–174, Nov. 2017.
[3] Y. Li, Y. Li, J. Cheng, and P. Wu, "Order assignment and scheduling for personal protective equipment production during the outbreak of epidemics," *IEEE Trans. Autom. Sci. Eng.*, vol. 19, no. 2, pp. 692–708, Apr. 2022.
[4] H. Ji and P. Wu, "Sailing route and speed optimization for green intermodal transportation," in *Proc. IEEE 5th Int. Conf. Intell. Transp. Eng. (ICITE)*, Sep. 2020, pp. 18–22.
[5] R. T. Marler and J. S. Arora, "The weighted sum method for multi-objective optimization: New insights," *Struct. Multidisciplinary Optim.*, vol. 41, no. 6, pp. 853–862, Jun. 2010.
[6] R. E. Steuer and E.-U. Choo, "An interactive weighted tchebycheff procedure for multiple objective programming," *Math. Program.*, vol. 26, no. 3, pp. 326–344, Oct. 1983.
[7] I. Das and J. E. Dennis, "Normal-boundary intersection: A new method for generating the Pareto surface in nonlinear multicriteria optimization problems," *SIAM J. Optim.*, vol. 8, no. 3, pp. 631–657, Aug. 1998.
[8] Q. Zhang and H. Li, "MOEA/D: A multiobjective evolutionary algorithm based on decomposition," *IEEE Trans. Evol. Comput.*, vol. 11, no. 6, pp. 712–731, Dec. 2007.
[9] S. Heng, D. Kim, T. Kim, and Y. Han, "How to solve combinatorial optimization problems using real quantum machines: A recent survey," *IEEE Access*, vol. 10, pp. 120106–120121, 2022.
[10] T. Morstyn, "Annealing-based quantum computing for combinatorial optimal power flow," *IEEE Trans. Smart Grid*, vol. 14, no. 2, pp. 1093–1102, Mar. 2023.
[11] E. Farhi, J. Goldstone, S. Gutmann, J. Lapan, A. Lundgren, and D. Preda, "A quantum adiabatic evolution algorithm applied to random instances of an NP-complete problem," *Science*, vol. 292, no. 5516, pp. 472–475, Apr. 2001.
[12] M. W. Johnson, M. H. S. Amin, S. Gildert, T. Lanting, F. Hamze, N. Dickson, R. Harris, A. J. Berkley, J. Johansson, P. Bunyk, E. M. Chapple, C. Enderud, J. P. Hilton, K. Karimi, E. Ladizinsky, N. Ladizinsky, T. Oh, I. Perminov, C. Rich, M. C. Thom, E. Tolkacheva, C. J. S. Truncik, S. Uchaikin, J. Wang, B. Wilson, and G. Rose, "Quantum annealing with manufactured spins," *Nature*, vol. 473, no. 7346, pp. 194–198, 2011.

[13] A. Lucas, "Ising formulations of many NP problems," *Frontiers Phys.*, vol. 2, p. 5, Feb. 2014.
[14] S. Matsubara, M. Takatsu, T. Miyazawa, T. Shibasaki, Y. Watanabe, K. Takemoto, and H. Tamura, "Digital annealer for high-speed solving of combinatorial optimization problems and its applications," in *Proc. 25th Asia South Pacific Design Autom. Conf. (ASP-DAC)*, Jan. 2020, pp. 667–672.
[15] C. Yoshimura, M. Hayashi, T. Takemoto, and M. Yamaoka, "CMOS annealing machine: A domain-specific architecture for combinatorial optimization problem," in *Proc. 25th Asia South Pacific Design Autom. Conf. (ASP-DAC)*, Jan. 2020, pp. 673–678.
[16] Y. Zhou, J. Wang, Z. Wu, and K. Wu, "A multi-objective Tabu search algorithm based on decomposition for multi-objective unconstrained binary quadratic programming problem," *Knowl.-Based Syst.*, vol. 141, pp. 18–30, Feb. 2018.
[17] J. Dubois-Lacoste, M. López-Ibáñez, and T. Stützle, "Improving the anytime behavior of two-phase local search," *Ann. Math. Artif. Intell.*, vol. 61, no. 2, pp. 125–154, Feb. 2011.
[18] M. Ayodele, R. Allmendinger, M. López-Ibáñez, and M. Parizy, "A study of scalarisation techniques for multi-objective QUBO solving," 2022, *arXiv:2210.11321*.
[19] M. Ayodele, R. Allmendinger, M. López-Ibáñez, A. Liefooghe, and M. Parizy, "Applying Ising machines to multi-objective QUBOs," in *Proc. Companion Conf. Genet. Evol. Comput.*, Jul. 2023, pp. 2166–2174.
[20] H. Nakayama, J. Koyama, N. Yoneoka, and T. Miyazawa, "Third generation digital annealer technology," Fujitsu, Kawasaki, Japan, Tech. Rep. DA_WP_EN_20210922, 2021. [Online]. Available: https://www.fujitsu.com/jp/documents/digitalannealer/researcharticles/
[21] K. Miettinen, *Nonlinear Multiobjective Optimization*, vol. 12. Berlin, Germany: Springer, 1999.
[22] H. Ishibuchi, N. Akedo, and Y. Nojima, "A study on the specification of a scalarizing function in MOEA/D for many-objective knapsack problems," in *Proc. 7th Int. Conf. Learn. Intell. Optim. (LION)*, Catania, Italy. Berlin, Germany: Springer, Jan. 2013, pp. 231–246.
[23] Y. Shang, "Scaled consensus and reference tracking in multiagent networks with constraints," *IEEE Trans. Netw. Sci. Eng.*, vol. 9, no. 3, pp. 1620–1629, May 2022.
[24] G. Kochenberger, J. K. Hao, F. Glover, M. Lewis, Z. Lü, H. Wang, and Y. Wang, "The unconstrained binary quadratic programming problem: A survey," *J. Combinat. Optim.*, vol. 28, no. 1, pp. 58–81, Jul. 2014.
[25] F. Glover, G. Kochenberger, and Y. Du, "A tutorial on formulating and using QUBO models," 2018, *arXiv:1811.11538*.
[26] L. While, P. Hingston, L. Barone, and S. Huband, "A faster algorithm for calculating hypervolume," *IEEE Trans. Evol. Comput.*, vol. 10, no. 1, pp. 29–38, Feb. 2006.

HIROSHI IKEDA received the B.S. and M.S. degrees in physics from Kyoto University, Japan, in 1992 and 1994, respectively. He joined Fujitsu Ltd., Japan, in 1994. Since 2009, he has been working in various fields with Fujitsu Laboratories Ltd., Japan, including statistical and mathematical modeling, financial engineering, and human posture recognition. He is currently a Researcher with Fujitsu Ltd., with a focus on combinatorial optimization as of 2021.

TAKASHI YAMAZAKI received the Doctor of Science degree from the Tokyo University of Science, Japan, in 2004. Since 1999, he has been conducting structural analysis at atomic resolution using transmission electron microscopy (TEM). From 2004 to 2008, he was a Research Assistant with the Tokyo University of Science. In 2008, he joined Fujitsu Laboratories, where he was engaged in the investigation of nanometer-scale quantitative analysis of electronic devices using TEM. Since 2009, he has been involved in the study of numerical optimization for quantitative analysis of analytical techniques. He is currently a Researcher with Fujitsu Ltd., Japan, primarily with a focus on the research and development of technology that applies numerical optimization to address real-world problems in the manufacturing field. In particular, he is actively promoting the construction of solutions for multi-objective optimization and the development of robust optimization techniques.